Journal of Colloid and Interface Science 579 (2020) 508–519

Contents lists available at ScienceDirect

Journal of Colloid and Interface Science

journal homepage: www.elsevier.com/locate/jcis

Magneto-mechanical actuation of barium-hexaferrite nanoplatelets for the disruption of phospholipid membranes

Tanja Goršak [a,b], Mitja Drab [c], Dejan Križaj [d], Marko Jeran [c,e], Julia Genova [f], Slavko Kralj [a], Darja Lisjak [a,b], Veronika Kralj-Iglič [e], Aleš Iglič [c], Darko Makovec [a,*]

[a] Department for Materials Synthesis, Jožef Stefan Institute, Jamova 39, SI-1000 Ljubljana, Slovenia
[b] Jožef Stefan International Postgraduate School, Jamova 39, SI-1000 Ljubljana, Slovenia
[c] Laboratory of Physics, Faculty of Electrical Engineering, University of Ljubljana, Tržaška 25, SI-1000 Ljubljana, Slovenia
[d] Laboratory of Bioelectromagnetics, Faculty of Electrical Engineering, University of Ljubljana, Tržaška 25, SI-1000 Ljubljana, Slovenia
[e] Laboratory of Clinical Biophysics, Faculty of Health Sciences, University of Ljubljana, Zdravstvena pot 5, SI-1000 Ljubljana, Slovenia
[f] Institute of Solid State Physics, Bulgarian Academy of Sciences, Tzarigradsko 72, 784 Sofia, Bulgaria

GRAPHICAL ABSTRACT

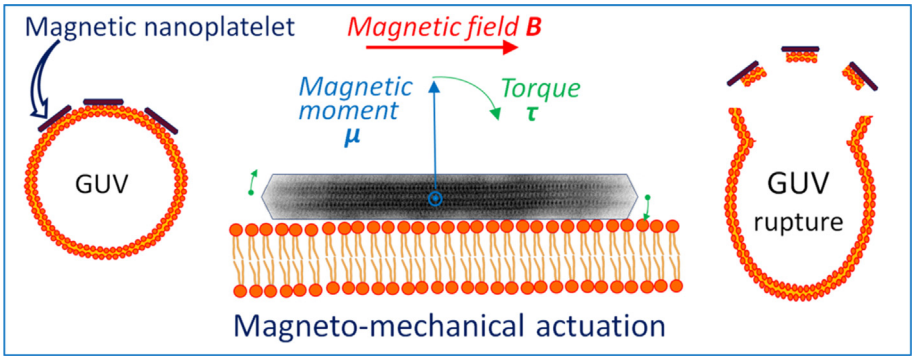

ARTICLE INFO

Article history:
Received 15 April 2020
Revised 1 June 2020
Accepted 18 June 2020
Available online 24 June 2020

Keywords:
Magneto-mechanical actuation
Hexaferrite nanoplatelets
Phospholipid membrane
Giant unilamellar vesicles
Theory

ABSTRACT

Hypothesis: The magneto-mechanical actuation (MMA) of magnetic nanoparticles with a low-frequency alternating magnetic field (AMF) can be used to destroy cancer cells. So far, MMA was tested on different cells using different nanoparticles and different field characteristics, which makes comparisons and any generalizations about the results of MMA difficult. In this paper we propose the use of giant unilamellar vesicles (GUVs) as a simple model system to study the effect of MMA on a closed lipid bilayer membrane, i.e., a basic building block of any cell.

Experiments: The GUVs were exposed to barium-hexaferrite nanoplatelets (NPLs, ~50 nm wide and 3 nm thick) with unique magnetic properties dominated by a permanent magnetic moment that is perpendicular to the platelet, at different concentrations (1–50 μg/mL) and pH values (4.2–7.4) of the aqueous suspension. The GUVs were observed with an optical microscope while being exposed to a uniaxial AMF (3–100 Hz, 2.2–10.6 mT).

Findings: When the NPLs were electrostatically attached to the GUV membranes, the MMA induced cyclic fluctuations of the GUVs' shape corresponding to the AMF frequency at the low NPL concentration

* Corresponding author.
E-mail address: darko.makovec@ijs.si (D. Makovec).

https://doi.org/10.1016/j.jcis.2020.06.079

(1 μm/mL), whereas the GUVs were bursting at the higher concentration (10 μg/mL). Theoretical considerations suggested that the bursting of the GUVs is a consequence of the local action of an assembly of several NPLs, rather than a collective effect of all the absorbed NPLs.

1. Introduction

Single-domain magnetic nanoparticles (MNPs) are the most promising mediators for remotely controlled nanomedicines. Unlike light, a magnetic field can penetrate into the tissue of a human body to a depth of more than 1 m without damping and distorting. The different interactions of the MNPs with the magnetic field (see the Supplementary Data for the general introduction) can be utilized for a variety of diagnostic and therapeutic modalities, including magnetic resonance imaging [1], magnetic particle imaging [2], magnetically targeted drug delivery [3], and cancer treatment with magnetic hyperthermia [4], or with magneto-mechanical actuation (MMA) [5–14]. The MMA treatment is based on the transfer of a mechanical force from the MNP on the cell. The force originates from the mechanical oscillations of the MNPs synchronized with an applied, low-frequency alternating magnetic field (AMF, frequency f < ~1 kHz). Aligning a MNP's magnetic moment $\boldsymbol{\mu}$ with the magnetic field $\boldsymbol{B}$ will result in rotational oscillations producing an effective torque $\boldsymbol{\tau_m} = \boldsymbol{\mu} \times \boldsymbol{B}$. In a inhomogeneous AMF the MNP will additionally experience translational oscillations due to the magnetic force $\boldsymbol{F_m}$ dragging it in the direction of the magnetic-field gradient $\nabla \boldsymbol{B}$ ($\boldsymbol{F_m} = (\boldsymbol{\mu} \cdot \nabla)\boldsymbol{B}$) [15,16]. The MMA does not include any thermal effects and has to be distinguished from the magnetic hyperthermia, which is based on the heating of MNPs in a radio-frequency AMF (f ~ 0.1–1 MHz) [15,16]. The hyperthermia method is already available as an experimental approach in oncological therapy [4].

Research on the control of cells and the regulation of cell events using MMA started in the late 20th century, initially using micron-sized magnetic particles, such as superparamagnetic microbeads [17–20]. The application of lithographically fabricated, ferromagnetic microdiscs with a spin-vortex ground state proved to be very effective for cancer-cell destruction [21–23]. Because of their small size, nanoparticles have many advantages for *in vivo* medical applications, when compared to larger, micron-sized particles, even though their magnetic moment $\boldsymbol{\mu}$ is much smaller ($\boldsymbol{\mu} = \boldsymbol{M}V$, where the magnetization $\boldsymbol{M}$ is defined by the selected magnetic material and V is the volume of the MNPs). MMA with MNPs was first applied for tissue engineering [24], although magnetic hyperthermia research also provided some hints. The actuation of MNPs with an AMF sometimes had effects on cancer cells that could not be related just to the heating, and so were ascribed to the MMA [5,6]. Only recently has the research on MMA intensified, mainly as a response to problems with hyperthermia cancer treatment, such as the ability to localize the heating to a small volume and, very important from the practical point of view, the high prices of magnetic applicators capable of producing sufficient amplitudes of AMF at radio frequencies. The prices of magnetic applicators operating at the low frequencies required for MMA are much lower.

Recently, various approaches were proposed for the destruction of different cancer cells using MNPs in combination with low-frequency AMF, both *in vitro* [7–12] and *in vivo* [13,14]. Generally, the authors reported a significant decrease in the cell viability and cell apoptosis [6,8,10–12].

Apart from the destruction of cancer cells, MMA was applied to manipulate the vital activity of cells by triggering individual mechanosensitive molecular structures, such as ion channels and receptors. For example, MMA was used to activate proliferation or differentiation signalling pathways in stem cells using the remote regulation of the receptors on the cell surfaces for regenerative medicine [25–27]. Moreover, MMA was successfully applied to trigger the drug release from different nano- and microcontainers [28–30]. For example, the actuation of MNPs adsorbed on GUVs with a low-frequency AMF increased the permeability of a phospholipid membrane and triggered the release of the load (fluorescent dye) from the vesicles [31].

In the above-mentioned previous studies, both translational and rotational oscillations were applied to actuate the MNPs with AMFs of different amplitude and with various spatial (homogeneous, field gradient) and time (uniaxial, rotating, or chaotic, at different frequencies) characteristics. In addition, MNPs with different magnetic properties, size, shape, surface functionalization, and state of agglomeration were studied for the MMA of different cells, which makes any generalization and comparison of the results difficult.

In this work we propose, for the first time, giant unilamellar vesicles (GUVs) as a model system to study MMA. The GUVs represent the simplest model of a cell membrane that first comes into contact with the nanoparticles. With a size ranging between 1 and 100 μm they can be simply visualized with optical microscopy techniques during the magnetic actuation [32]. The tests on the GUVs are much faster when compared to the tests on cell cultures and can be used for simple screening of the field and the evaluation of the MNP characteristics with regard to the efficiency of the MMA. In addition, the state of the MNP agglomeration and the interactions between the nanoparticles and the membrane are much more easily assessed in the GUV suspension than in a cell culture.

Iron-oxide maghemite (γ-Fe_2O_3) MNPs are preferred in medicine, mainly because they are considered safe and were approved by the US Food and Drug Administration for *in vivo* applications [33]. However, the magnetic properties of the maghemite are far from ideal for applications based on MMA. In this work, permanently magnetic barium-hexaferrite nanoparticles with an attractive combination of platelet shape and a unique, perpendicular orientation of $\boldsymbol{\mu}$, were tested for the first time in MMA. Barium hexaferrite exhibits a highly anisotropic hexagonal magnetoplumbite structure. Its growth is limited in the c-direction, meaning that the crystals grow in the form of thin platelets, with the magnetic easy axis pointing in the direction of the crystallographic c-axis [34]. Due to a large uniaxial magnetocrystalline anisotropy (K_1-$\approx$ 33 kJ/m^3) the magnetic dipole of a nanoplatelet $\boldsymbol{\mu}$ also remains fixed in the c-axis when the hexaferrite is synthesized in the form of small platelet nanoparticles, i.e., nanoplatelets (NPLs), meaning that the $\boldsymbol{\mu}$ points perpendicular to the platelet [35]. This unique magnetic property of the hexaferrite NPLs has already led to some novel applications, such as ferromagnetic liquids [36–38], magneto-optical composites [39], and novel spin-memory devices [40,41]. In medicine, hexaferrite NPLs have enabled the development of high-contrast cardiovascular imaging based on magnetically modulated optical coherence tomography and MRI [42].

In this work we studied the MMA disruption of the phospholipid membranes of GUVs using non-agglomerated hexaferrite NPLs (~50 nm wide and 3 nm thick) at a well-defined AMF (uniaxial, f = 3–100 Hz, B = 2.2–10.6 mT).

2. Experimental

2.1. Preparation of nanoplatelet suspensions

The Sc-substituted barium-hexaferrite NPLs [43] were synthesized hydrothermally [44]. The materials used are listed in the Supplementary Data. In brief, an aqueous solution of Ba^{2+}, Fe^{3+}, and Sc^{3+} nitrates was rapidly mixed into aqueous NaOH to co-precipitate the corresponding hydroxides. The slurry was then heated to 240 °C in a closed Inconel autoclave.

The NPLs were coated with dextran in stable aqueous suspensions in several steps [45]. In the first step, citric acid was adsorbed onto the NPLs to electrostatically stabilize the starting suspension. The citric acid was adsorbed onto the NPLs in the suspension where the pH was set to 5.1 with aqueous ammonia at 80 °C. The excess citric acid was removed with sedimentation of the NPLs using centrifugation. Then the citric-acid-coated NPLs were washed and re-dispersed in a diluted ammonia solution at pH 10.1. In the next step, the NPLs were coated with a thin layer of silica by hydrolysis and the polycondensation of tetraethyl orthosilicate (TEOS) on the surfaces of the citric-acid-adsorbed NPLs in a water/ethanol suspension [46]. The coating reaction was catalysed by the addition of aqueous ammonia. Finally, the dextran molecules (MW ca. 20,000 Da) were covalently grafted onto the surfaces of the silica-coated NPLs using the 3-glycidyloxypropyl-trimethoxysilane (GLYMO) linker. First, the epoxy ring of the GLYMO was reacted with the alcohol groups of the dextran in aqueous sodium hydroxide. The product of the GLYMO-dextran reaction was purified by dialysis against deionized water and grafted onto the surfaces of the silica-coated NPLs via the reaction of their methoxysilane groups with the silanol groups, which are present on the silica surface. The final suspensions were colloidally stable, even in complex biological media [45]. The dextran-grafted NPLs are referred to as HF-DEX.

To modify the surface charge of the NPLs, a mixture of 90% dextran and 10% (3-aminopropyl)triethoxysilane (APS) was also grafted onto the NPLs surfaces (the NPLs HF-DEX+). The APS contains amino groups, which provide a positive surface charge on the NPLs [47].

2.2. Formation of giant unilamellar vesicles

The GUVs were prepared using a modified electroformation method [48] from 1-palmitoyl-2-oleoyl-*sn-glycero*-3-phosphocholine (POPC) or l-stearoyl-2-oleoyl-*sn-glycero*-3-phosphocholine (SOPC) (the materials used are listed in the Supplementary Data). A stock solution of POPC or SOPC (1 mg/mL) was prepared by dissolving the dry lipid in chloroform. The phospholipid solution (40 μL) was applied over two platinum electrodes and the chloroform was allowed to evaporate for 2 h under vacuum. The coated electrodes were then placed 2 mm apart in an electroformation vessel, containing 2 mL of 0.3 mol/L sucrose solution at pH = 7.0. An alternating electric field of magnitude 5 V/mm and frequency of 10 Hz was applied to the electrodes overnight. In the morning, the magnitude and frequency of the alternating electric field were gradually reduced at intervals of 15 min, first to 2.5 V/mm and 5 Hz, then to 2.5 V/mm and 2.5 Hz, and finally to 1 V/mm and 1 Hz. After the electroformation, the vesicles were taken from the same electroformation vessel and diluted with a 0.3 mol/L glucose solution in the volume ratio 1:3, while maintaining the original pH of the solution.

2.3. Characterization

The NPLs were characterized using a transmission electron microscope (TEM Jeol 2010F) and a probe spherical-aberration corrected (C_S) scanning-transmission electron microscope (STEM Jeol ARM 200CF). The NPL widths were estimated from the TEM images with a visual measurement using DigitalMicrograph™ Gatan Inc. software. The magnetic properties of the NPLs were measured with a vibrating-sample magnetometer (VSM, Lakeshore 7407) after they were aligned in the magnetic field. The NPLs were hydrophobized by the adsorption of ricinoleic acid onto their surfaces and then a low concentration of the NPLs was homogeneously dispersed in a liquid wax heated to 80 °C. After the NPLs were aligned with the homogeneous magnetic field (H = 1000 kA/m) the wax was solidified by cooling to retain the texture.

The hydrodynamic size of the NPLs in suspension (at a concentration of 0.1 mg/mL) was measured with dynamic light scattering (DLS Fritsch, Analysette 12 DynaSizer).

The zeta-potential was measured in suspensions of NPLs (~0.1 mg/mL) in a 0.3 mol/L glucose solution as a function of the pH using a ZetaPALS instrument (Brookhaven Instruments Corporation). The pH of the suspension was set with NaOH for measurements at a higher pH, and separately, with HCl at lower pH values. For the measurement of the zeta-potential, a GUVs suspension after electroformation in a sucrose solution was diluted with a glucose solution and the pH was set to the desired value with HCl or NaOH. The measurements were independently repeated at least three times. However, due to the poor stability and the large size of the GUVs (more than 5 μm) the results of the zeta-potential measurements should be taken with special care [49,50]. The measurements of the GUVs were verified by measurements of the POPC unilamellar vesicles (LUVs) [51] with a diameter of ~0.1 μm, prepared by extrusion [52]. The values obtained with the GUVs matched those of the LUVs, within the expected experimental uncertainty of the method.

2.4. Magneto-mechanical actuation

The GUVs were exposed to magnetic nanoplatelets (HF-DEX or HF-DEX+) with the final concentration of the NPLs ranging from 1 μg/mL to 50 μg/mL and the pH was adjusted to an exact value with diluted HCl (pH = 4.2, 5.2, or 7.0). The suspension of GUVs with NPLs was then exposed to a uniaxial, homogeneous AMF at various frequencies (f = 3–100 Hz) and amplitudes (B = 2.2–10.6 mT). The solutions of the GUVs with added NPLs were monitored with a phase-contrast optical microscope (Nikon Eclipse te2000-s) while exposed to the AMF (see the Supplementary Data, Fig. S1). To quantify the effect of MMA, the GUV/NPL suspensions were exposed to the AMF for fixed periods of time (10 min in most of the experiments) and subsequently analysed with the microscope. The stock suspension of NPLs (7 mg/mL) in a 0.3-mol/L glucose solution was added to the GUV suspension to set the final NPLs concentration ranging from 1 to 50 μg/mL. For a single experiment, 1 mL of the GUV suspension with NPLs was prepared. The sample was divided into four parts: one part, i.e., the control, was not exposed to the AMF, while the other three parts were exposed to three different conditions of AMF, for example, three different frequencies. After the magnetic treatment, 200 μL from each part was pipetted into one of the four perfusion chambers. The suspensions were then allowed to sediment for 30 min before recording began. Two video tracks were recorded in each chamber for individual analyses. During recording, the focus was being simultaneously adjusted. Each video track was approximately 2.5 min long (3000 frames), with a per-pixel spatial resolution of 0.25 mm (video image resolution of 5.7 megapixels). The number of GUVs in every treated suspension was estimated by counting the GUVs from the videos and comparing to the estimation for the untreated suspension. At least 200 GUVs were counted for an individual estimation. Each experiment was repeated three times, and the average values are presented. For the estimation of the

GUVs' size distributions, the areas of the GUVs were taken from the video images using DigitalMicrograph™ Gatan Inc. software. The size expressed as an equivalent diameter was estimated for all the GUVs recorded close to the focus.

2.5. Bending elastic constant measurements

The suspension of HF-DEX+ NPLs was added to the aqueous suspension of GUVs. The final pH was around 5.4. The fluctuating GUVs with and without NPLs were observed under a phase-contrast microscope (Axiovert 100, Zeiss, Germany, oil-immersion objective Ph3 with 100 × magnification). A double-channel thermostatic equipment was used to precisely control the temperature of the experimental table and around the objective to be 30 °C. An image of a selected GUV was acquired every second and recorded until the total number of images was approximately 400. The GUV contour determination, the mean-squared-amplitudes calculation and the fitting procedures to determine the bending elastic modulus (k_c) were performed as described in [53]. The bending elasticity modulus was calculated as a weighted average value of 5 vesicles.

3. Experimental results and discussion

3.1. Hexaferrite nanoplatelets

Fig. 1(a) shows a TEM image of the dextran-grafted silica-coated nanoplatelets HF-DEX. The hexaferrite core of the hexagonal NPLs is coated with a thin, approximately 2-nm-thick, uniform amorphous silica layer, clearly visible when the NPL is oriented edge on, with the large surfaces parallel to the electron beam (Fig. 1 (b)). Due to the low density compared to that of the inorganic materials, the dextran grafted on the NPL surfaces is not visible on the TEM images. The width of the NPLs was estimated from the TEM images to be 52 ± 12 nm (Fig. 1(c)). The thickness of the NPLs is, however, defined by their unique structure at 3.0 nm, while only a minor part of the NPLs was 4.2 nm thick [54]. Thus, for the silica-coated NPLs, the thickness ranged from 7 to 10 nm.

The NPLs exhibited strongly anisotropic magnetic properties with a broad magnetic hysteresis loop (i.e., a high coercivity H_C ~ 142 kA/m) when measured with the magnetic field applied perpendicular to the platelets and a much narrower loop when measured parallel to the platelets (Fig. 1(d)). The saturation magnetization (M_S) for the synthesized hexaferrite NPLs was 40 Am^2/kg. After the coating with nonmagnetic silica and dextran the M_S of HF-DEX NPLs decreased to 29 Am^2/kg.

3.2. Interactions between giant unilamellar vesicles and nanoplatelets in the suspensions

The NPLs were added to GUVs suspended in a glucose solution and exposed to the homogeneous AMF. The GUVs had a broad size distribution, with diameters ranging from 2 to 50 μm (Fig. 2(a)).

The force that can be produced by MNPs in an AMF depends greatly on their size, which can change drastically with agglomeration before or during the MMA. DLS measurements showed no agglomeration of the NPLs in the glucose solution used for the MMA experiments (see Fig. S2 in the Supplementary Data). No agglomeration was detected after the addition of the NPLs to the GUVs and after the exposure to the AMF: no agglomerates were observed by optical microscope and neither was there any visual evidence for sedimentation of the NPLs.

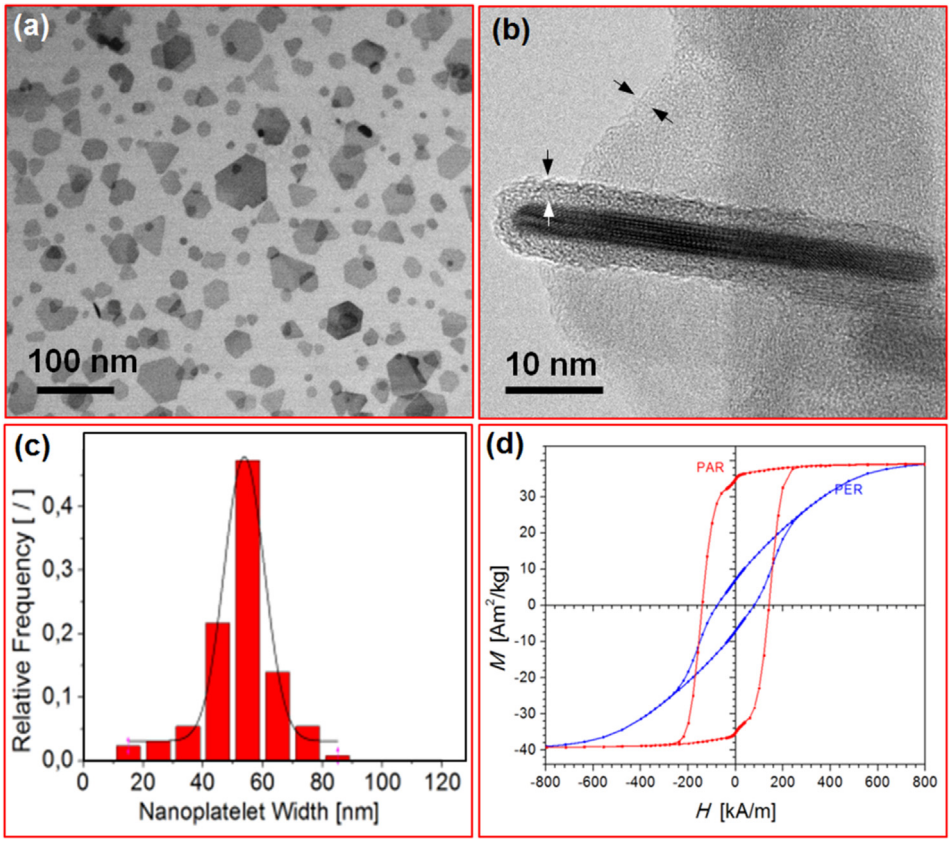

Fig. 1. BF STEM image of dextran-grafted and silica-coated HF-DEX nanoplatelets lying flat on the specimen support (a) and TEM image of the nanoplatelet oriented edge-on (b). The silica coating is marked with arrows. (c) Distribution of nanoplatelet widths expressed as an equivalent effective diameter. (d) Magnetic hysteresis loops for hexaferrite nanoplatelets measured perpendicular (PER) and parallel (PAR) to their magnetic easy axes.

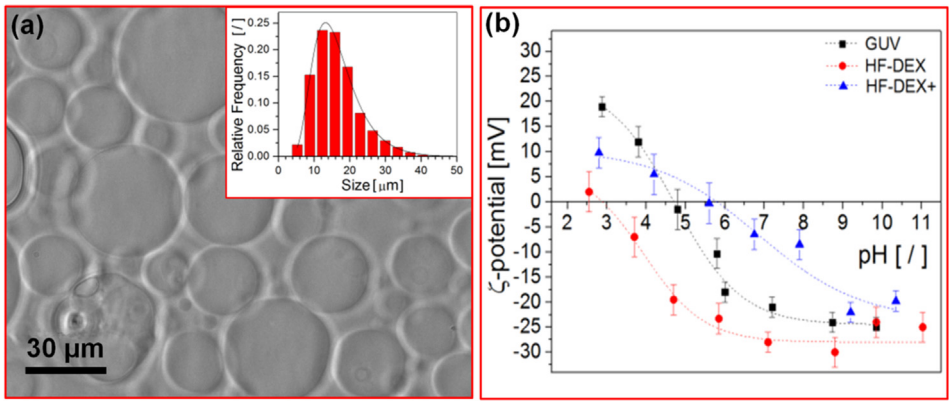

Fig. 2. (a) Optical micrograph of GUVs (inset: distribution of GUV size) and (b) zeta-potential as a function of pH for suspensions of GUVs and NPLs HF-DEX and HF-DEX+ suspended in a 0.3 mol/L aqueous glucose solution.

The transfer of the force depends critically on the interactions between the MNP and the membrane. In an aqueous suspension the NPLs can interact with the GUV membrane via electrostatic interactions. The GUVs were prepared from POPC, which is a zwitterion molecule with a head-group containing an anionic phosphate and a cationic quaternary ammonium group, rendering the net charge of the molecule neutral. However, this does not exclude the attractive interactions between the zwitterionic lipid bilayer and the negatively charged nanoparticles, as shown in [55,56]. Fig. 2(b) shows the zeta-potential of the GUVs as a function of the pH of the suspension. The GUVs exhibit a positive zeta-potential at a pH below the isoelectric point (IEP) of pH ~ 4.7 and a relatively large negative zeta-potential at neutral pH. The HF-DEX NPLs show a negative zeta-potential above the IEP at pH ~ 3. Attractive or repulsive interactions can therefore exist between the HF-DEX and the GUVs; below or above pH ~ 4.7, respectively. With grafting the mixed layer of the positively charged APS molecules and the dextran molecules the IEP of the HF-DEX+ NPLs shifts to a higher pH of ~5.6. The interactions between the HF-DEX+ and the GUVs are therefore attractive in the range from approximately pH ~ 4.7 to pH ~ 5.6 and repulsive outside this pH range. Due to the attractive electrostatic interactions the NPLs adhere on the GUVs' membranes. The adsorption of NPLs onto the GUVs in the suspensions with prevailing attractive interactions between the particles is also suggested from TEM analysis. When such suspensions were dried on the TEM specimen support, the NPLs deposited in the form of patches of a specific, circular shape (see Figs. S3 and S4). The circular shape clearly originates from the adsorption of the NPLs onto the GUVs before the deposition (see the Supplementary Data for details).

The membrane bending constant (k_c) significantly decreases after the adhesion of the NPLs to the GUV membranes. At the NPL concentration of 1 µg/mL the k_c of the POPC membrane of the GUVs decreased by about one-third (from $1.3 \pm 0.1 \cdot 10^{-19}$ J to $0.86 \pm 0.28 \cdot 10^{-19}$ J). This result is in agreement with previous experimental results with other types of nanoparticles [57] and also with theoretical predictions for the small area density of the adhered nanoparticles. Namely, the theoretical predictions suggest that the adsorption of plate-like nanoparticles [58], elongated inclusions [59] and other types of isotropic and anisotropic adhered nanoparticles at small concentrations can "soften" the GUV membrane [59–70], making it prone to magneto-mechanical disintegration.

In our case the adhesion of the negatively charged, plate-like NPLs to the surface of the zwiterionic (dipolar) POPC or SOPC GUVs is accompanied by a more perpendicular average orientation of the lipid head-groups [55,56], as shown in Fig. 3. This can lead to more tightly packed, raft-like lipid domains below the NPL adhesion area with increased local rigidity, while the lipid regions away from the adhered nanoparticle can be softened due to the decreased area density of the lipids [65]. It is, therefore, expected that at a small area density of the adhered NPLs the membrane's bending modulus is decreased, while it is increased at higher values of the area density of the NPLs. The influence of the adhered nanoparticles on the rigidity of the GUV membrane is further discussed in the Supplementary Data [64–76].

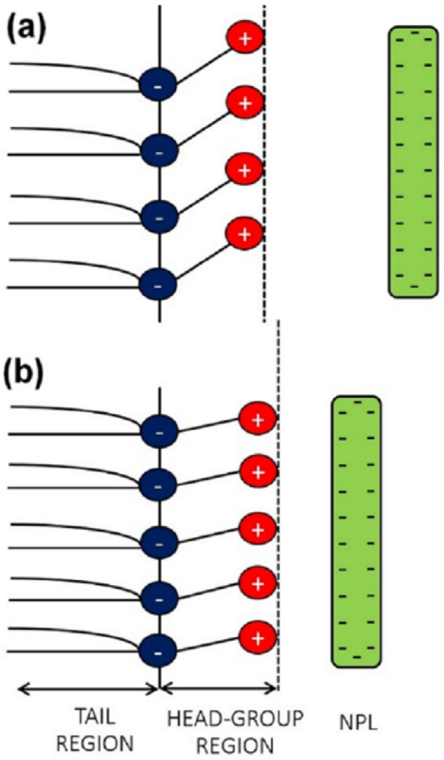

Fig. 3. Schematic presentation of the average lipid dipolar (zwitterionic) head-group orientation as a function of the distance from the negatively charged, plate-like NPL, as predicted by molecular dynamics simulations and statistical thermodynamics modelling [55,56]. At smaller distances the average orientation of the lipid head-groups changes from inclined (panel (a)) to more perpendicular (panel (b)) (see [55,56] for details).

3.3. Giant unilamellar vesicles and nanoplatelets exposed to an alternating magnetic field

To test the magneto-mechanical effect, the NPLs were added to the suspension of GUVs at different pH values and at different concentrations. The HF-DEX NPLs were added to the GUVs at pH = 7.4, where both exhibited a negative surface charge (repulsive interaction), and at pH = 4.2, where the GUVs were positively charged and the HF-DEX NPLs were negatively charged, leading to attractive interactions. The HF-DEX+ NPLs were added to the GUV suspension at pH = 7.4 (repulsive interactions) and at pH = 5.2 (attractive interactions).

The suspension of GUVs with NPLs was monitored with a phase-contrast optical microscope while being exposed to the AMF. No effect of the AMF on the GUVs was detected in the case of repulsive interactions, i.e., when the GUVs were exposed to the NPLs at pH = 7.4. However, when the GUVs and the NPLs exhibited the opposite charge (GUVs exposed to HF-DEX at pH = 4.2 or to HF-DEX+ at pH = 5.2), the effect of the MMA was clearly visible. The effect varied depending on the NPL concentration. When the NPLs concentration was low, i.e., 1 μg/mL, the GUVs' shape cyclically fluctuated with the frequency of the field. This effect was only visible at low AMF frequencies, below 10 Hz (Video 1 is given in the Supplementary Data). When the NPL concentration was larger, i.e., at 10 μg/mL, some of the GUVs ruptured only when exposed to the AMF. The rupturing was clearly a consequence of the MMA of the NPLs adhered to the GUV membrane. Fig. 4 shows the time lapse of a large vesicle bursting and resulting in many smaller endovesicles in its interior (HF-DEX at 10 μg/mL, pH = 5.2, B = 7 mT, f = 3 Hz). The upper-left image with $t = 0$ marks the start of the experiment, when the AFM was switched on. After a few seconds, the outer membrane of the vesicle ruptured due to the magneto-mechanical effect of the NPLs (the Video 2 is given in the Supplementary Data, see also Videos 3 and 4).

The observed dependence of the effect of actuated NPLs on the pH value of the GUVs suspension can be directly related to the interactions between the NPLs and the GUV membranes. When the NPLs and the GUV surfaces in the aqueous suspension exhibited the same sign of the surface charge (pH = 7.4), the NPLs did not adhere to the membrane and the force produced by the NPLs' actuation could not be transferred to the GUV. Only the opposite surface charge enabled the firm adherence of the NPLs, which enabled the efficient transfer of the torque to the membrane.

To evaluate the influence of the magnetic field parameters on the efficiency of the NPLs' actuation, the number of GUVs was determined from videos recorded before and after the treatment with the AMF. The relative number of GUVs after the treatment was obtained by normalization with respect to the number of GUVs in the untreated suspensions. When the GUVs without the NPLs at pH values of 7.4, 5.2, and 4.2 were treated with AMFs of different B/f and for different times, the relative number of GUVs fluctuated within 20% (Fig. 5). This was ascribed to the manipulation, e.g., rupturing during pipetting, sedimentation during experiment, and counting error. Thus, 20% was set as the expected uncertainty of the experiments. When the GUVs were exposed to the HF-DEX or HF-DEX+ NPLs at pH 7.4 (the same sign of surface charge), the relative number of GUVs remained within 20% of the measurement after the treatment with the AMF (Fig. 5). Due to the repulsive electrostatic interactions between the NPLs and the GUV membranes, there was no transfer of force from the NPLs to the GUVs. However, when the GUVs were exposed to the HF-DEX NPLs at pH = 4.2 or to HF-DEX+ at pH = 5.2 (i.e., an attractive interaction), the relative number of GUVs significantly decreased with the treatment. The relative number of GUVs varied with the frequency (Fig. 5), amplitude (Fig. 6(a)) and the duration of the treatment (Fig. 6(b)). For example, the treatment of the GUVs exposed to HF-DEX NPLs (10 μg/mL) with an AMF of B = 7.0 mT for 10 min resulted in the decrease in the relative GUV numbers by approximately 35%, 50%, and 40% at 3 Hz, 10 Hz, and 100 Hz, respectively (Fig. 5). The relative number of GUVs also decreased with B (Fig. 6(a)) and the duration of the treatment (Fig. 6(b)).

4. Theoretical considerations

In order to obtain a deeper insight into the mechanism that leads to the disruption of the phospholipid bilayer, the relevant forces were analysed. Since the experiments were conducted in the low-frequency regime (3–100 Hz), global resonant effects were ruled out as possible culprits for the GUV's rupture. The speed of

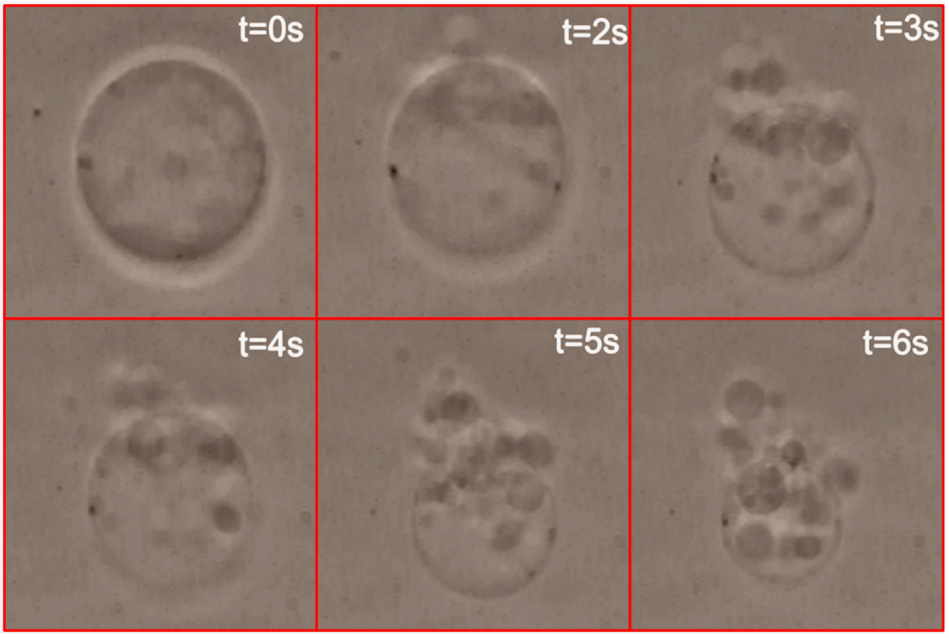

Fig. 4. Time lapse image of a GUV with HF-DEX+ NPLs exposed to AMF (B = 7 mT, f = 3 Hz).

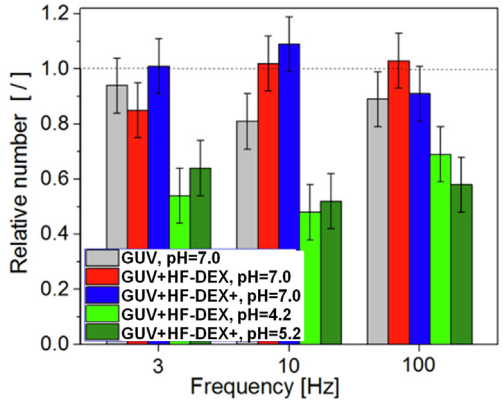

Fig. 5. Relative number of GUVs after they were exposed to different NPLs (HF-DEX or HF-DEX+, 0.01 mg/ml) for different pH values of the suspension (pH = 7.0, 5.2, 4.2) and treated with the AMF (10 min, B = 7.0 mT) at different frequencies (3, 10 and 100 Hz).

sound propagation in the lipid membranes is of the order of 100 m/s [77], which is many orders of magnitude faster than the perturbations induced by the oscillating particles.

The dynamics of free-floating MNPs in an AMF were studied before [78,79]. In the absence of an external field the particles have random spatial orientations. At very low concentrations (10 μg/mL) of the NPLs in the suspensions applied in our experiments the magnetic dipole interactions can be neglected, so the particles do not disturb one another's motion while floating freely. The average interaction energy can be estimated to be $W_{D-D} \approx \mu_0 \mu^2 / 2\pi r^3$, and this is negligible compared to the AMF interaction energy $W_{AMF} = \mu B_0$, with r being the average distance between neighboring dipoles. When the homogeneous AMF is switched on, it acts on the particles with a torque $\boldsymbol{\tau} = \boldsymbol{\mu} \times \boldsymbol{B}$, whose magnitude depends on the angle φ between $\boldsymbol{\mu}$ and $\boldsymbol{B}$ in the cross product $\mu B \sin\varphi$. Since the AMF's $\boldsymbol{B}$ is dependent on time and oscillates with an angular frequency Ω, the magnitude of the torque also changes periodically: $\tau = \mu B_0 \sin\varphi \sin\Omega t$. Here, B_0 is the amplitude of the AMF. In a viscous medium with viscosity η, the counteracting torque can be approximated by a torque on a sphere rotated at a constant angular velocity. From Stokes' equations for incompressible fluids, this can be shown to be equal to $6\eta V_{hd}\dot{\varphi}$ after a short derivation (given, for example, in [80]). Here, $\dot{\varphi}$ marks the angular velocity of the spinning NPL and V_{hd} is the hydrodynamic spherical volume of the NPL. The equation of motion for a free-rotating NPL is then

$$J\ddot{\varphi} = \mu B_0 \sin\varphi \sin\Omega t - 6\eta V_{hd}\dot{\varphi}. \quad (1)$$

The moment of inertia J of the used NPLs can be estimated and is of the order of 10^{-35} kgm^2, many orders of magnitude smaller than the interaction energy μB_0. Inertial effects are therefore negligible, which means the particles reach their terminal velocities instantaneously. We are left with the equation

$$\dot{\varphi} = \omega \sin\varphi \sin\Omega t, \quad (2)$$

where $\omega = \mu B_0 / 6\eta V_{hd}$ is the ratio of the driving to the viscous effects governing the dynamics. The solutions to Eq. (2) are wholly determined by the ratio of the AMF frequency Ω to ω, the latter being medium specific. When $\Omega \ll \omega$, the particle undergoes periodic and sudden 180° "flips" following the direction of AMF. At a frequency $\Omega \geq \omega$, the viscosity becomes dominant and the particles oscillate nearly harmonically with decreasing amplitudes at increasing Ω.In the limit of very large AMF frequencies, the particles cannot follow the alternating field and completely stop oscillating.

When NPLs are added to a suspension of GUVs, some particles adsorb to the outer membrane of the GUVs due to their opposite electrostatic charge. Let us consider a single NPL attached to a GUV membrane. We assume that the most energetically favourable way of adhering the NPLs to the GUV is planar, with the base of the NPL in contact with the membrane; it is improbable that the NPL firmly attaches to the membrane with its edge. We assume that once the particle is adsorbed onto the lipid membrane, it can move only laterally but not medially (across the thickness of the lipid bilayer). We also assume that the NP cannot unbind itself or flip without causing a mechanical rupture.

When the AMF field is switched on, the NPL is bound to follow the field and oscillate, locally bending the membrane, but the membrane pulls it back into position. The equation of particle dynamics is similar to Eq. (2), with the addition of another term that accounts for the bent membrane trying to return to its equilibrium, unperturbed position (Fig. 7). This additional counteracting torque can be accounted for by a greater effective viscosity η, rendering the parameter ω smaller. A previous study by Golovin et al. [78] assumed that such a paddle-like motion of the particle normal to the membrane increases the pressure underneath it, which can be estimated by considering the maximum force F on the membrane [78]:

$$F \approx \frac{\mu B_0}{L}, \quad (3)$$

where L is the dimension of the particle. The authors of [78] estimate this force to be of the order of 10 pN at $B_0 = 100$ mT (for rod-like magnetite MNPs with diameters of 30 nm, saturation magnetization 80 Am^2/kg and density 5400 kg/m^3), which results in an additional stress on the membrane of approximately 40 kPa, argu-

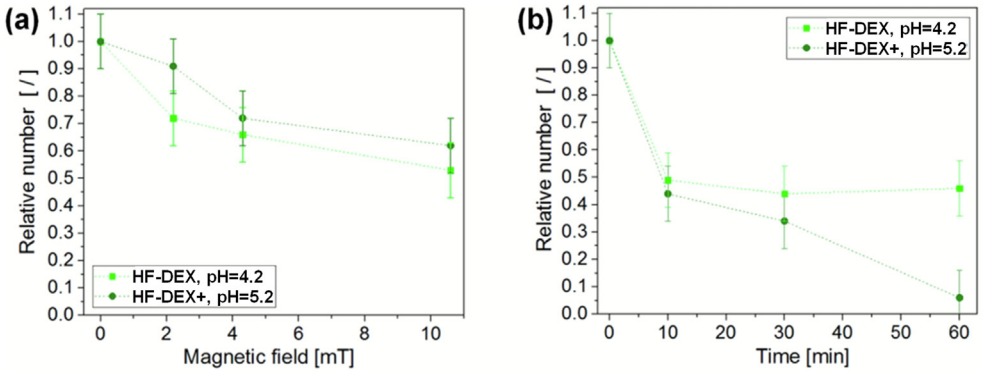

Fig. 6. Relative number of GUVs after treatment with the AMF as a function of magnetic field B (f = 10 Hz, t = 10 min) (a) and as a function of treatment duration (f = 10 Hz, B = 10.5 mT) (b). The GUVs were treated with HF-DEX NPLs at pH = 4.2 and with HF-DEX+ NPLs at pH 5.2.

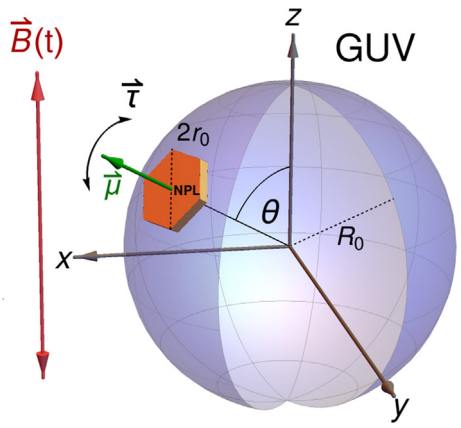

Fig. 7. Schematic of a NPL at a polar angle Θ attached to the outer membrane of a GUV with exaggerated proportions. The radius of the GUV is R_0, while the effective radius of the NPL is r_0. The AMF, shown with the red arrow, pulls and pushes the NPL into and from the GUV membrane, locally increasing its lateral tension σ. A symmetric situation applies to NPLs that adsorb with the magnetic moment pointing inwards. (For interpretation of the references to colour in this figure legend, the reader is referred to the web version of this article.)

ing that this is several times higher than the normal membrane rigidity and therefore sufficient for significant membrane damage. We see two major problems with this hypothesis. First, the authors assume that the cell is ruptured by a force normal to the membrane, which is an insufficient explanation. Even though the exact mechanism of membrane failure is unknown, it is widely observed that membrane strength is closely related to the membrane elasticity, characterized by the area-expansion modulus, not taken into account with mere normal forces (see, e.g., [81]). Secondly, the value of 40 kPa cited in [78] was adapted from an experiment where an AFM cantilever arm was penetrating a trapped leukaemia cell (see [82]). Such a method of cell penetration is not related to the local effect of a single nanoparticle in an oscillatory motion. The mechanisms are hardly identical and the result of the former cannot be simply transferred to the latter.

Since the area expansion modulus is dependent on the membrane tension, we chose to focus on the differences in the lateral tension in our theoretical descriptions. We presume that the rupture mechanism does not rely on forces normal to the membrane, but rather on lateral tensile forces that tear the membrane and induce vesicle collapse.

With these considerations in mind, we presume that the oscillating motion of the membrane-adsorbed MNPs in the AMF locally deforms the lipid membrane, inducing the loss of integrity or membrane-pore formation. In its equilibrium state, the GUV's shape is determined by the minimum of the bending energy and assumes a negligible surface tension. With local perturbations and bending due to the adsorbed NPLs, the surface tension of the membrane is increased in proportion to the maximum amplitude of the adsorbed oscillating particles. Experiments conducted on GUVs pressed against pointed, nanostructured surfaces found that the additional lateral tension required to mechanically rupture a GUV vary between $\sigma_{burst} = 4 - 7\text{mN/m}$ [83]. We rely heavily on this result in the following estimations, setting it as our main reference point for a threshold beyond which GUVs rupture reliably.

We can estimate the maximum excess lateral tension imposed by the membrane-attached NPL with a short calculation, available in the Supplementary Data, Appendix B. For this reason, we postulate that the lateral tension in the membrane in its relaxed state of the GUV is negligible. The shape of the membrane is wholly determined by the minimization of its bending energy, which is proportional to its curvature. The final result for the extra lateral tension σ induced in the membrane for a NPL with radius r_0, (derived in Supplementary Data, B) yields:

$$\sigma = \frac{\mu B_0}{\pi r_0^2}. \tag{4}$$

It is important to note that a larger NPL has a proportionately larger magnetic moment relative to its radius $\mu \propto {r_0}^2$. Considering that the saturation magnetization M_S for the synthesized hexaferrite NPLs used in the experiments was 40 Am^2/kg, an estimation for the largest NPL with radius $r_0 = 50$ nm with a magnetic dipole moment of $\mu = 6.6 \cdot 10^{-18}$ Am^2 in an AMF with amplitude $B_0 = 7$ mT gives a value of $\sigma = 0.006$ mN/m, which is three orders of magnitude less than σ_{burst}, which is in the range 4–7 mN/m [83].

It is therefore improbable to think that a single attached NPL could rupture the membrane in the AMF. However, if more particles gather on the membrane in an assembly of multiple NPLs as a result of magnetic attraction, the net magnetic moment in equation (4) is increased. Conversely, the effective radius of such an assembly grows slower than its net magnetic moment, since the NPLs stack up most conveniently in an overlapping manner. Adhered onto the membrane, such an assembly has an increased potential for reaching the threshold for bursting σ_{burst}. As an illustrative example, let us consider an assembly of 10 NPLs – approximately on top of each other with double the effective radius – will induce a three-fold increase in the lateral tension to $\sigma =$ 0.06 mN/m in comparison to only one NPL ($\sigma = 0.006$ mN/m). An assembly of 100 NPLs stuck to the region of the GUV with an effective radius of $r_0 = 100$ nm could reach tensions up to $\sigma = 0.15$ mN/m. It is not known how large these assemblies could be, but given that the average number of NPLs in one mL is of the order 10^{13}–10^{15}, they could potentially become numerous.

Given that more than one NPL or one assembly of NPLs is adsorbed onto each GUV at any time, exceeding the maximum surface tension due to the collective oscillation of the particles is even more probable. If additive, an oscillating particle pulling on the membrane at one end increases the lateral tension of the membrane throughout the GUV. In the simplest example, two neighbouring NPLs double the excess tension σ in the membrane whether they rotate in the same or opposite directions (Fig. 8).

Assuming the excess-surface-tension effect is indeed collective, we can again estimate the increase in σ by considering the NPLs, or the assemblies of NPLs side by side in a collective effect, covering only the circumference of the GUV. Consider that the entire circumference of the GUV is covered at the "equator", at a polar angle of 90° (see Fig. 7). The circumference around the GUV is equal to $2\pi R_0$ and the NPL effective diameter $2r_0$, meaning that hypothetically it can accommodate a total of $\pi R_0/r_0$ NPLs positioned side by side. When they all oscillate in the external AFM simultaneously, the collective lateral tension σ_{total} can be estimated by the simple multiplication of Eq. (4) with the number of NPLs$\pi R_0/r_0$:

$$\sigma_{total} = \frac{R_0 B_0 \mu}{r 3_0}. \tag{5}$$

Using the same parameter values as before ($\mu = 6.6 \cdot 10^{-18}$ Am^2, $r_0 = 50$ nm $B_0 = 7$mT) and R_0 =1–25 μm, the tension σ_{total} is in the range 0.4–9.2 mN/m, which is of the same order of magnitude of σ_{burst}. Seeing that the proportionality of $\mu \propto {r_0}^2$ now no longer holds, due to the third power in the denominator, the upper bound for σ_{total} can theoretically become even larger, up to 92 mN/m for smallest particles with $r_0 = 5$ nm and $\mu = 6.6 \cdot 10^{-20}$Am^2.

The upper bound confirms that the collective effect is indeed more than sufficient to rupture the GUV membrane according to [83]. In reality we expect that more NPLs are found around the GUV at other polar angles (Fig. 7) that are not 90°, further contributing to the effect.

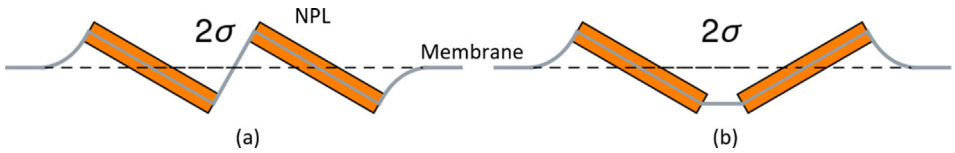

Fig. 8. Two neighbouring NPLs increase the lateral tension by a factor of 2, whether their magnetic dipole moments μ point in the same (a), or different directions (b).

It is interesting to note the dependence of the lateral tension σ_{total} on the GUV radius R_0 (Eq. (5)). If larger GUVs are more susceptible to bursting due to the more adhered NPLs providing more rotational torque, it seems that the number of larger GUVs will be lower after the MMA is mediated with the NPLs. We tested this hypothesis experimentally by determining the GUV size distributions before and after the exposure to the AMF and found that there is no particular tendency for the larger GUVs to burst more frequently (Fig. 9), meaning that the mechanism for GUV bursting does not favour scaling, but rather that all sizes are similarly susceptible to rupturing.

We therefore concluded that lone NPLs cannot rupture the membrane. Additionally, the experiments deny that a collective effect could be the main cause of membrane bursting, since we would then observe a significant decrease in the number of the largest GUVs. It seems most probable that the excess bursting tension σ_{burst} is achieved by an oscillation of assemblies of NPLs adhered to the membrane. It is likely that the NPLs are inhomogeneously distributed over the GUV membranes, with areas of higher surface coverage being the locations where membrane disruption can be initiated. However, additional experiments are needed to research the NPL distribution over the GUVs.

5. General discussion

The reported research gives reliable experimental evidence that a MMA can be used to disrupt phospholipid-bilayer membranes, even for relatively small sizes of non-agglomerated MNPs relevant for *in vivo* medical applications, such as magneto-mechanical cancer therapy. Lysosome membrane damage causing the extravasation of lysosomal contents into the cytoplasm was most frequently reported as the likely cause of cell death during MMA [6,8,10–12]. From a general therapeutic-delivery aspect, the nanoparticles must be smaller than 200 nm to avoid the body's complement immune system from quickly removing them from the blood stream. The nanoparticles with a size of about 50 nm usually show the greatest cellular uptake [84]. At a given size suitable for *in-vivo* applications, the main factors influencing the efficiency of MMA are the shape and magnetic properties of the MNPs and the interactions of the MNPs with the membrane. To enable the efficient transfer of mechanical force the MNP has to be firmly attached to the membrane. For the tests on GUVs the nanoparticles can simply be electrostatically absorbed onto the membrane. The electrostatic interactions can be controlled by grafting different charged molecules onto the MNP surfaces or by changing the properties of the suspension, such as the pH. However, with numerous (bio)molecules and ions abundant in biological fluids the control of electrostatic interactions between the colloidal particles is limited in more realistic tests on cells. The adsorption of protein corona on the nanoparticle surface can strongly reduce the nanoparticle adhesion to the membrane [85]. However, the specific molecules can be conjugated onto the MNP surfaces to enable their bonding with the membrane. For example, antibodies targeting the lysosomal protein marker LAMP1 were conjugated to MNPs to enable their attachment to the lysosome membranes [8]. In addition, certain proteins or other types of molecules with a distinct internal charge distribution in biological fluids can induce the mediated attractive interactions between like-charged surfaces [86–88].

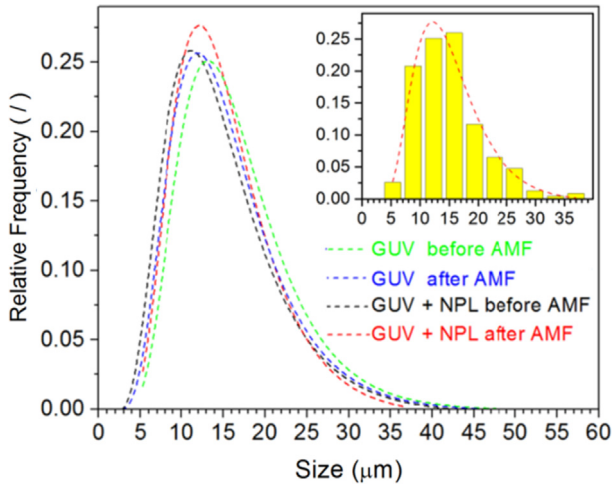

Fig. 9. Size distribution of GUVs with and without NPLs (HF-DEX+, pH = 5.2), before and after exposure to AMF (f = 10 Hz, B = 7mT, t = 10 min). The empirical size distributions measured from optical micrographs were fitted with lognormal curves (see inset) and compared. No significant changes in the size distribution suggests a local, rather than a global effect of increased surface tension.

The force produced by rotational oscillations in a homogeneous AMF will only be efficiently transferred to the membrane if the MNPs exhibit an anisotropic shape. Due to a large contact surface between the MNP and the membrane, the plate-like shape is preferred. However, for these plate-like MNPs the symmetry of the magnetic anisotropy is of crucial importance [89]. Even for a soft-magnetic material, like the frequently used iron oxide maghemite, the shape of these MNPs will not be effective in the homogeneous AMF. Due to a low, cubic magnetocrystalline anisotropy of maghemite ($K_I \approx 5$ kJ/m^3) [34] the magnetic moments $\boldsymbol{\mu}$ of such plate-like MNPs will orient in-plane. With the in-plane orientation of $\boldsymbol{\mu}$ the plate-like MNPs will align with the large surfaces parallel to the field vector. In contrast, the plate-like MNPs with a perpendicular $\boldsymbol{\mu}$ will orient perpendicular to the field and continuously flip with the alternations of $\boldsymbol{B}$, which is an optimal situation for the transfer of torque to the membrane. Moreover, the shape (anisotropic and isotropic), molecular structure, electric charge and area density of the attached MNPs are also important for a decrease in the membrane bending constant after the attachment of the MNPs to the GUV membrane [58–65,67–70]. The hexaferrite NPLs are actually a very rare example of platelet nanoparticles with such a perpendicular orientation of $\boldsymbol{\mu}$ [90].

6. Conclusions

The actuation of magnetic nanoparticles with a low-frequency alternating magnetic field, i.e., magneto-mechanical actuation (MMA), can be applied to exert physical force on different biological structures, such as a lipid bilayer membrane. We used giant unilamellar vesicles (GUVs) as a model system, for the first time, to study the effect of magneto-mechanical actuation. In summary,

the GUVs were exposed to barium-hexaferrite nanoplatelets (NPLs), approximately 50 nm wide and 3 nm thick. The NPLs differ from the magnetic nanoparticles of soft-magnetic materials (e.g., iron oxide) that were previously used for the MMA [7–14], as they exhibited permanent magnetic moments pointing perpendicular to the platelet. The colloidal stability of the NPL suspension was ensured with covalent grafting of dextran-based molecules onto their surfaces, previously coated with a thin silica layer. The surface charge on the NPLs was controlled by the composition of the grafted molecular layer (dextran, a mixture of dextran and 3-aminopropyl silane) and with the suspension's pH. When the NPLs exhibited the opposite surface charge to the GUVs they adsorbed onto the membranes. The actuation of the NPLs attached onto the membrane resulted in cyclic fluctuations of the GUVs' shape, corresponding to the AMF frequency at low NPL concentrations (1 μm/mL) and the bursting of the GUVs at higher concentrations (10 μg/ml), where both examples were given at relatively modest magnetic-field amplitudes, below 10 mT. Theoretical considerations suggested that the GUV's bursting was due to the local action of an assembly of several NPLs and not due to the collective effect of all the NPLs absorbed on the GUV. The study evidenced that MMA efficiently disrupted the membrane, even with small magnetic nanoparticles, suitable for in-vivo medical applications, providing that the particles are of an appropriate platelet shape and with the right magnetic properties.

The GUVs proved to be an efficient and relatively flexible model system (when compared to cell models) to study the MMA. They enable investigations of the interactions between the phospholipid membranes, magnetic nanoparticles and an alternating magnetic field under defined experimental conditions and can therefore be used for screening the different nanoparticles and field characteristics for applications based on MMA.

CRediT authorship contribution statement

Tanja Goršak: Investigation, Conceptualization, Methodology, Visualization, Writing - original draft. **Mitja Drab:** Formal analysis, Visualization, Writing - original draft, Writing - review & editing. **Dejan Križaj:** Resources, Supervision. **Marko Jeran:** Investigation. **Julia Genova:** Investigation, Writing - original draft. **Slavko Kralj:** Investigation. **Darja Lisjak:** Supervision. **Veronika Kralj-Iglič:** Formal analysis, Methodology, Supervision. **Aleš Iglič:** Conceptualization, Formal analysis, Supervision, Writing - original draft, Writing - review & editing. **Darko Makovec:** Conceptualization, Methodology, Visualization, Supervision, Data curation, Project administration, Writing - original draft, Writing - review & editing.

Declaration of Competing Interest

The authors declare that they have no known competing financial interests or personal relationships that could have appeared to influence the work reported in this paper

Acknowledgments

The support of the Slovenian Research Agency (ARRS) within the Project L2-8166, P2-0232 and P3-0388 is acknowledged. We also acknowledge the CENN Nanocenter for the use of VSM equipment. We would like to acknowledge the fruitful discussions with Dr. S. Čopar and Dr. A. Kregar.

Appendix A. Supplementary data

Supplementary data to this article can be found online at https://doi.org/10.1016/j.jcis.2020.06.079.

References

[1] R. Weissleder, M. Nahrendorf, M.J. Pittet, Imaging macrophages with nanoparticles, Nat. Mater. 13 (2014) 125–138.
[2] B. Gleich, J. Weizenecker, Tomographic imaging using the nonlinear response of magnetic particles, Nature 435 (2005) 1214–1217.
[3] S. Kralj, T. Potrc, P. Kocbek, S. Marchesan, D. Makovec, Design and fabrication of magnetically responsive nanocarriers for drug delivery, Curr. Med. Chem. 24 (2017) 454–469.
[4] K. Maier-Hauff, F. Ulrich, D. Nestler, H. Niehoff, P. Wust, B. Thiesen, H. Orawa, V. Budach, A. Jordan, Efficacy and safety of intratumoral thermotherapy using magnetic iron-oxide nanoparticles combined with external beam radiotherapy on patients with recurrent glioblastoma multiforme, J. Neurooncol. 103 (2011) 317–324.
[5] M. Creixell, A.C. Bohorquez, M. Torres-Lugo, C. Rinaldi, EGFR-targeted magnetic nanoparticle heaters kill cancer cells without a perceptible temperature rise, ACS Nano 5 (2011) 7124–7129.
[6] M. Domenech, I. Marrero-Berrios, M. Torres-Lugo, C. Rinaldi, Lysosomal membrane permeabilization by targeted magnetic nanoparticles in alternating magnetic fields, ACS Nano 7 (2013) 5091–5101.
[7] H.L. Jia, C. Wang, Y. Li, Y. Lu, P.P. Wang, W.D. Pan, T. Song, Combined effects of 50 Hz magnetic field and magnetic nanoparticles on the proliferation and apoptosis of PC12 cells, Biomed. Environ. Sci. 27 (2014) 97–105.
[8] E. Zhang, M.F. Kircher, M. Koch, L. Eliasson, S.N. Goldberg, E. Renström, Dynamic magnetic fields remote-control apoptosis via nanoparticle rotation, ACS Nano 8 (2014) 3192–3201.
[9] M.F. Contreras, R. Sougrat, A. Zaher, T. Ravasi, J. Kosel, Non-chemotoxic induction of cancer cell death using magnetic nanowires, Int. J. Nanomed. 10 (2015) 2141–2153.
[10] A.M. Master, P.N. Williams, N. Pothayee, N. Pothayee, R. Zhang, H.M. Vishwasrao, Y.I. Golovin, J.S. Riffle, M. Sokolsky, A.V. Kabanov, Remote actuation of magnetic nanoparticles for cancer cell selective treatment through cytoskeletal disruption, Sci. Rep. 6 (2016) 33560.
[11] S. Hapuarachchige, Y. Kato, E.J. Ngen, B. Smith, M. Delannoy, D. Artemov, Non-temperature induced effects of magnetized iron oxide nanoparticles in alternating magnetic field in cancer cells, PLOS ONE (2016). https://doi.org/10.1371/journal.pone.0156294.
[12] Y. Shen, C. Wu, T.Q. Uyeda, G.R. Plaza, B. Liu, Y. Han, M.C. Lesniak, Y. Cheng, Elongated nanoparticle aggregates in cancer cells for mechanical destruction with low frequency rotating magnetic field, Theranostics 7 (2017) 1735–1748.
[13] A. Vegerhof, E.A. Barnoy, M. Motiei, D. Malka, Y. Danan, Z. Zalevsky, R. Popovtzer, Targeted magnetic nanoparticles for mechanical lysis of tumor cells by low-amplitude alternating magnetic field, Materials 9 (2016). 943-1–943-12.
[14] Y. Chen, P. Han, Y. Wu, Z. Zhang, Y. Yue, W. Li, M. Chu, Hedgehog-like gold-coated magnetic microspheres that strongly inhibit tumor growth through magnetomechanical force and photothermal effects, Small 14 (2018).
[15] Y.I. Golovin, S.L. Gribanovsky, D.Y. Golovin, N.L. Klyachko, A.G. Majouga, A.M. Master, M. Sokolsky, A.V. Kabanov, Towards nanomedicines of the future: remote magneto-mechanical actuation of nanomedicines by alternating magnetic fields, J. Control. Release 219 (2015) 43–60.
[16] Y.I. Golovin, A.O. Zhigachevb, M.V. Efremova, A.G. Majouga, A.V. Kabanov, N.L. Klyachko, Ways and methods for controlling biomolecular structures using magnetic nanoparticles activated by an alternating magnetic field, Nanotechnol. Russ. 13 (2018) 295–304.
[17] J.L. Kirschvink, Constraints on biological effects of weak extremely low-frequency electromagnetic fields—comment, Phys. Rev. A 46 (1992) 2178–2184.
[18] H. Pommerenke, E. Schreiber, F. Durr, B. Nebe, C. Hahnel, W. Moller, J. Rychly, Stimulation of integring receptors using a magnetic drag force device induces an intracellular free calcium response, Eur. J. Cell Biol. 70 (1996) 157–164.
[19] E.A. Vitol, V. Novosad, E.A. Rozhkova, Multifunctional ferromagnetic disks for modulating cell function, IEEE Trans. Magn. 48 (2012) 3269–3274.
[20] J. Chen, B. Fabry, E.L. Schiffrin, N. Wang, Twisting integrin receptors increases endothelin-1 gene expression in endothelial cells, Am. J. Physiol. Cell Physiol. 280 (2001) 1475–1484.
[21] D.-H. Kim, E.A. Rozhkova, I.V. Ulasov, S.D. Bader, T. Rajh, M.S. Lesniak, V. Novosad, Biofunctionalized magnetic-vortex microdiscs for targeted cancer-cell destruction, Nat. Matter. 9 (2010) 165–171.
[22] D.-H. Kim, P. Karavayev, E.A. Rozhkova, J. Pearson, V. Yefremenko, S.D. Bader, V. Novosad, Mechanoresponsive system based on sub-micron chitosan-functionalized ferromagnetic disks, J. Mater. Chem. 21 (2011) 8422–8426.
[23] Y. Cheng, M.E. Muroski, D.C. Petit, R. Mansell, T. Vemulkar, R.A. Morshed, Y. Han, I.V. Balyasnikova, C.M. Horbinski, X. Huang, L. Zhang, R.P. Cowburn, M.S. Lesniak, Rotating magnetic field induced oscillation of magnetic particles for in vivo mechanical destruction of malignant glioma, J. Control. Release 223 (2016) 75–84.
[24] J. Dobson, Remote control of cellular behaviour with magnetic nanoparticles, Nat. Nanotechnol. 3 (2008) 139–143.
[25] C. Wu, Y. Shen, M. Chen, K. Wang, Y. Li, Y. Cheng, Recent advances in magnetic-nanomaterial-based mechanotransduction for cell fate regulation, Adv. Mater. 30 (2018) 1705673.
[26] M. Rotherham, A.J. El Haj, Remote activation of the Wnt/β-catenin signalling pathway using functionalised magnetic particles, PLoS ONE 10 (2015) e0121761.

[27] J.R. Henstock, M. Rotherham, H. Rashidi, K.M. Shakesheff, A.J. El Haj, Remotely activated mechanotransduction via magnetic nanoparticles promotes mineralization synergistically with bone morphogenetic protein 2: applications for injectable cell therapy, Stem Cells Transl. Med. 3 (2014) 1363–1674.
[28] Z. Lu, M.D. Prouty, Z. Guo, V.O. Golub, C.S. Kumar, Y.M. Lvov, Magnetic switch of permeability for polyelectrolyte microcapsules embedded with Co Au nanoparticles, Langmuir 21 (2005) 2042–2050.
[29] S. Nappini, F.B. Bombelli, M. Bonini, B. Norden, P. Baglioni, Magnetoliposomes for controlled drug release in the presence of low-frequency magnetic field, Soft Matter 6 (2010) 154–162.
[30] S. Nappini, M. Bonini, F.B. Bombelli, F. Pineider, C. Sangregorio, P. Baglioni, B. Norden, Controlled drug release under a low frequency magnetic field: effect of the citrate coating on magnetoliposomes stability, Soft Matter 7 (2011) 1025–1037.
[31] S. Nappini, T. Al Kayal, D. Berti, B. Norden, P. Baglioni, Magnetically triggered release from giant unilamellar vesicles: visualization by means of confocal microscopy, J. Phys. Chem. Lett. 2 (2011) 713–718.
[32] G. Beaune, B. Dubertret, O. Clement, C. Vayssettes, V. Cabuil, C. Menager, Giant vesicles containing magnetic nanoparticles and quantum dots: feasibility and tracking by fiber confocal fluorescence microscopy, Angew. Chem. Int. Ed. 46 (2007) 5421–5424.
[33] T.K. Thanh Nguyen, Magnetic Nanoparticles from Fabrication to Clinical Applications, CRC Press, Boca Raton, FL, 2012, pp. 65–78.
[34] J.P. Smit, H.P.J. Wjin, Ferrites: Physical Properties of Ferrimagnetic Oxides in Relation to their Technical Applications, first ed., N.V. Phipips, Eindhoven, 1959.
[35] B. Belec, G. Dražić, S. Gyergyek, B. Podmiljšak, T. Goršak, M. Komelj, J. Nogués, D. Makovec, Novel Ba-hexaferrite structural variations stabilized on the nanoscale as building blocks for epitaxial bi-magnetic hard/soft sandwiched maghemite/hexaferrite/maghemite nanoplatelets with out-of-plane easy axis and enhanced magnetization, Nanoscale 9 (2017) 17551–17560.
[36] A. Mertelj, D. Lisjak, M. Drofenik, M. Čopič, Ferromagnetism in suspensions of magnetic plate-lets in liquid crystal, Nature 504 (2013) 237–241.
[37] R. Sahoo, M.V. Rasna, D. Lisjak, A. Mertelj, S. Dhara, Magnetodielectric and magnetoviscosity response of a ferromagnetic liquid crystal at low magnetic fields, Appl. Phys. Lett. 106 (2015) 161905-1–161905-4.
[38] P.J. Ackerman, I.I. Smalyukh, Static three-dimensional topological solutions in fluid chiral ferromagnets and colloids, Nat. Mater. 16 (2016) 426.
[39] G. Ferk, P. Kranjc, A. Hamler, A. Mertelj, F. Cebollada, M. Drofenik, D. Lisjak, Monolithic mag-neto-optical nanocomposites of barium hexaferrite platelets in PMMA, Sci. Rep. 5 (2015) 11395-1–11394-8.
[40] H. Al-Bustami, G. Koplovitz, D. Primc, S. Yochelis, E. Capua, D. Porath, R. Naaman, Y. Paltiel, Single nanoparticle magnetic spin memristor, Small 14 (2018) 1801249.
[41] G. Koplovitz, D. Primc, O.B. Dor, Y. Shira, D. Rotem, D. Porath, Y. Paltiel, Magnetic nanoplatelet-based spin memory device operating at ambient temperatures, Adv. Mater. 29 (2017) 1606748.
[42] J. Hu, T. Gorsak, E. Martín Rodríguez, D. Calle, T. Muñoz-Ortiz, D. Jaque, N. Fernández, L. Cussó, F. Rivero, R. Aguilar Torres, J. García Solé, A. Mertelj, D. Makovec, M. Desco, D. Lisjak, F. Alfonso, F. Sanz-Rodríguez, D.H. Ortgies, Magnetic nanoplatelets for high contrast cardiovascular imaging by magnetically modulated optical coherence tomography, ChemPhotoChem 3 (2019) 1–12.
[43] D. Makovec, M. Komelj, G. Dražić, B. Belec, T. Goršak, S. Gyergyek, D. Lisjak, Incorporation of Sc into the structure of barium-hexaferrite nanoplatelets and its extraordinary finite-size effect on the magnetic properties, Acta Mater. 172 (2019) 84e91.
[44] D. Lisjak, M. Drofenik, Chemical substitution: an alternative strategy for controlling the particle size of barium ferrite, Cryst. Growth Des. 12 (11) (2012) 5174–5179.
[45] T. Goršak, D. Makovec, U. Javornik, B. Belec, S. Kralj, D. Lisjak, A functionalization strategy for the dispersion of permanently magnetic barium-hexaferrite nanoplatelets in complex biological media, Colloids Surfaces A Physicochem. Eng. Asp. 573 (2019) 119–127.
[46] S. Kralj, D. Makovec, S. Čampelj, M. Drofenik, Producing ultra-thin silica coatings on iron-oxide nanoparticles to improve their surface reactivity, J. Magn. Magn. Mater. 322 (2010) 1847–1853.
[47] S. Čampelj, D. Makovec, M. Drofenik, Functionalization of magnetic nanoparticles with 3-aminopropyl silane, J. Mag. Mag. Mater. 321 (2009) 1346–1350.
[48] M.I. Angelova, S. Soléau, P. Méléard, F. Faucon, P. Bothorel, Preparation of giant vesicles by external AC electric fields. Kinetics and applications, Trends Colloid. Interface. Sci. VI 131 (1992) 127–131.
[49] K. Carvalho, L. Ramos, C. Roy, C. Picart, Biophys. Giant unilamellar vesicles containing phosphatidylinositol(4,5)bisphosphate: characterization and functionality, Biophys. J. 95 (2008) 4348–4360.
[50] J. Steinkühler, P. De Tillieux, R.L. Knorr, R. Lipowsky, R. Dimova, Charged giant unilamellar vesicles prepared by electroformation exhibit nanotubes and transbilayer lipid asymmetry, Sci. Rep. 8 (2018) 11838.
[51] H.A. Faizi, S.L. Frey, J. Steinkühler, R. Dimova, P.M. Vlahovska, Bending rigidity of charged lipid bilayer membranes, Soft Matter 15 (2019) 6006–6013.
[52] T. Bayburt, M.H. Gelb, Interfacial catalysis by human 85 kDa cytosolic phospholipase A2 on anionic vesicles in the scooting mode, Biochemistry 36 (1997) 3216–3231.
[53] J. Genova, M. Mitov, Measuring bending elasticity of lipid bilayers, in: A. Iglič, J. Genova (Eds.), Advances in Planar Lipid Bilayers and Liposomes, Elsevier, London, 2013, pp. 1–27.
[54] D. Makovec, B. Belec, T. Goršak, D. Lisjak, M. Komelj, G. Dražić, S. Gyergyek, Discrete evolution of the crystal structure during the growth of Ba-hexaferrite nanoplatelets, Nanoscale 10 (2018) 14480–14491.
[55] A. Velikonja, P.B. Santhosh, E. Gongadze, M. Kulkarni, K. Eleršič, Š. Perutkova, V. Kralj-Iglič, N. Poklar Ulrih, A. Iglič, Interaction between dipolar lipid headgroups and charged nanoparticles mediated by water dipoles and ions, Int. J. Mol. Sci. 14 (2013) 15312–15329.
[56] E. Gongadze, A. Velikonja, Š. Perutkova, P. Kramar, A. Maček-Lebar, V. Kralj-Iglič, A. Iglič, Ions and water molecules in an electrolyte solution in contact with charged and dipolar surfaces, Electrochim. Acta 126 (2014) 42–60.
[57] P.B. Santhosh, A. Velikonja, Š. Perutkova, E. Gongadze, M. Kulkarni, J. Genova, K. Eleršič, A. Iglič, V. Kralj Iglič, N. Poklar Ulrich, Influence of nanoparticle-membrane electrostatic interactions on membrane fuidity and bending elasticity, Chem. Phys. Lipids 178 (2014) 52–62.
[58] A. Iglič, T. Slivnik, V. Kralj-Iglič, Elastic properties of biological membranes influenced by attached proteins, J. Biomech. 40 (2007) 2492–2500.
[59] H. Bouvrais, P. Méléard, T. Pott, K.J. Jensen, J. Brask, J.H. Ipsen, Softening of POPC membranes by magainin, Biophys. Chem. 137 (2008) 7–12.
[60] V. Kralj-Iglič, V. Heinrich, S. Svetina, B. Žekš, Free energy of closed membrane withanisotropic inclusions, Eur. Phys. J. B 10 (1999) 5–8.
[61] I. Bivas, P. Méléard, Bending elasticity and bending fluctuations of lipid bilayer containing an additive, Phys. Rev. E 67 (2003) 012901.
[62] V. Kralj-Iglič, S. Svetina, B. Žekš, Shapes of bilayer vesicles with membrane embedded molecules, Eur. Biophys. J. 24 (1996) 311–321.
[63] H. Agrawal, M. Zelisko, L. Liu, P. Sharma, Rigid proteins and softening of biological membranes with application to HIV-induced cell membrane softening, Sci. Rep. 6 (2016) 25412.
[64] I. Hoffmann, R. Michel, M. Sharp, O. Holderer, M.-S. Appavou, F. Polzer, B. Farago, M. Gradzielski, Softening of phospholipid membranes by the adhesion of silica nanoparticles–as seen by neutron spin-echo (NSE), Nanoscale 6 (2014) 6945–6952.
[65] A. Bhat, L.W. Edwards, X. Fu, D.L. Badman, S. Huo, A.J. Jin, Q. Lu, Effects of gold nanoparticles on lipid packing and membrane pore formation, Appl. Phys. Lett. 109 (2016) 263106.
[66] M. Fošnarič, K. Bohinc, D.R. Gauger, A. Iglič, V. Kralj-Iglič, S. May, The influence of anisotropic membrane inclusionson curvature elastic properties of lipid membranes, J. Chem. Inf. Model. 45 (2005) 1652–1661.
[67] M. Fošnarič, A. Iglič, S. May, Influence of rigid inclusions on the bending elasticity of a lipid membrane, Phys. Rev. E 74 (2006) 051503.
[68] P. Méléard, T. Pott, H. Bouvrais, J.H. Ipsen, Advantages of statistical analysis of giant vesicle flickering for bending elasticity measurements, Eur. Phys. J. E 34 (2011) 116.
[69] K.I. Pakkanen, L. Duelund, K. Qvortrup, J.S. Pedersen, J.H. Ipsen, Mechanics and dynamics of triglyceride-phospholipid model membranes: implications for cellular properties and function, Biochim. Biophys. Acta, Biomembr. 2011 (1808) 1947–1956.
[70] H. Bouvrais, Bending Rigidities of Lipid Bilayers: their determination and main inputs in biophysical studies, in: A. Iglič (Ed.), Advances in planar lipid bilayers and liposomes, 2012, pp. 1–75.
[71] R. Dimova, Recent developments in the field of bending rigidity measurements on membranes, Adv. Colloid Interface Sci. 208 (2014) 225–234.
[72] S.T. Milner, S.A. Safran, Dynamic fluctuations of droplet microemulsions and vesicles, Phys. Rev. A 36 (1987) 4371–4379.
[73] S. Penič, A. Iglič, I. Bivas, M. Fošnarič, Bending elasticity of vesicle membranes studied by Monte Carlo simulations of vesicle thermal shape fluctuations, Soft Matter 11 (2015) 5004–5009.
[74] L. Bo, R.E. Waugh, Determination of bilayer membrane bending stiffness by tether formation from giant, thin-walled vesicles, Biophys. J. 55 (1989) 509–517.
[75] E. Evans, W. Rawicz, Entropy-driven tension and bending elasticity in condensed-fluid membranes, Phys. Rev. Lett. 64 (1990) 2094–2097.
[76] P. Méléard, C. Gerbeaud, P. Bardusco, N. Jeandaine, M.D. Mitov, L. Fernandez-Puente, Mechanical properties of model membranes studied from shape transformations of giant vesicles, Biochimie 80 (1998) 401–413.
[77] J. Griesbauer, A. Wixforth, M.F. Schneider, Wave propagation in lipid monolayers, Biophys. J. 97 (2009) 2710–2716.
[78] Y.I. Golovin, S.L. Gribanovsky, D.Y. Golovin, A.O. Zhigachev, N.L. Klyachko, A.G. Majouga, M. Sokolsky, A.V. Kabanov, The dynamics of magnetic nanoparticles exposed to non-heating alternating magnetic field in biochemical applications: theoretical study, J. Nanopart. Res. 19 (2017) 59-1–59-14.
[79] X.J. Janssen, A.J. Schellekens, K. van Ommering, L.J. van Izendoorn, M.W. Prins, Controlled torque on superparamagnetic beads for functional biosensors, Biosens. Bioelectron. 24 (2009) 1937–1941.
[80] É. Guazzelli, J. Morris, S. Pic, A Physical introduction to suspension dynamics (Cambridge Texts in Applied Mathematics), Cambridge University Press, Cambridge, 2011.
[81] D.V. Zhelev, Material property characteristics for lipid bilayers containing lysolipid, Biophys. J. 75 (1998) 321–330.
[82] W.A. Lam, M.J. Rosenbluth, D.A. Fletcher, Chemotherapy exposure increases leukemia cell stiffness, Blood 109 (2007) 3505–3508.
[83] S. Cheeseman, V.K. Truong, V. Walter, F. Thalmann, C.M. Marques, E. Hanssen, J. Vongsvivut, M.J. Tobin, V.A. Baulin, S. Juodkazis, S. Maclaughlin, G. Bryant, R.J. Crawford, E.P. Ivanova, Interaction of giant unilamellar vesicles with

the surface nanostructures on dragonfly wings, Langmuir 35 (2019) 2422–2430.
[84] N. Hoshyar, S. Gray, H. Han, G. Bao, The effect of nanoparticle size on *in vivo* pharmacokinetics and cellular interaction, Nanomedicine (Lond.) 11 (2016) 673–692.
[85] A. Lesniak, A. Salvati, M.J. Santos-Martinez, M.W. Radomski, K.A. Dawson, C. Åberg, Nanoparticle adhesion to the cell membrane and its effect on nanoparticle uptake efficiency, J. Am. Chem. Soc. 135 (2013) 1438–1444.
[86] J. Urbanija, K. Bohinc, A. Bellen, S. Maset, A. Iglič, V. Kralj-Iglič, P.B.S. Kumar, Attraction between negatively charged surfaces mediated byspherical counterions with quadrupolar chargedistribution, J. Chem. Phys. 129 (2008) 105101.
[87] J. Zelko, A. Iglič, V. Kralj-Iglič, P.B.S. Kumar, Effects of counter ion size on the attraction between similarly charged surfaces, J. Chem. Phys. 133 (2010) 204901.
[88] J. Gimsa, P. Wysotzki, Š. Perutkova, T. Weihe, P. Elter, P.E. Marszalek, V. Kralj-Iglič, A. Iglič, The spermidine-induced attraction of like-charged surfaces is correlated with the pH-dependent spermidine charge: force spectroscopy characterization, Langmuir 34 (2018) 2725–2733.
[89] R. Mansell, T. Vemulkar, D.C.M.C. Petit, Y. Cheng, J. Murphy, M.S. Lesniak, R.P. Cowburn, Magnetic particles with perpendicular anisotropy for mechanical cancer cell destruction, Sci. Rep. 7 (2017) 4257.
[90] D. Lisjak, A. Mertelj, Anisotropic magnetic nanoparticles: a review of their properties, syntheses and potential applications, Prog. Mater Sci. 95 (2018) 286–328.